Reconfigurable Physical Unclonable Function Based on Spin-Orbit Torque Induced Chiral Domain Wall Motion

Zhen Cao, Shuai Zhang, Jian Zhang, Nuo Xu, *Member, IEEE*, Ruofan Li, Zhe Guo, Jijun Yun, Min Song, Qiming Zou, Li Xi, Oukjae Lee, Xiaofei Yang, Xuecheng Zou, *Senior Member, IEEE*, Jeongmin Hong, and Long You, *Senior Member, IEEE*

***Abstract*— A reliable design of physical unclonable function (PUF) based on spin-orbit torque (SOT) induced domain wall (DW) motion has been proposed and experimentally demonstrated. Magnetic DWs are nucleated and propagate in Ta/CoFeB/MgO heterostructures in which their device-to-device variation enables the PUF, while cycle-to-cycle variation in DW motion enables the reconfigurable design. Furthermore, field-free SOT switching has been observed in the chiral domain wall likely caused by the large Dzyaloshinskii-Moriya interaction (DMI) effect. The proposed DW motion based anti-counterfeiting device shows good promises as a CMOS-compatible PUF for hardware security.**

***Index Terms*— PUF, SOT, DW motion, security.**

I. Introduction

PHYSICAL unclonable functions (PUFs) utilize process variations and physical stochastics to generate unique binary code, which are unclonable and unpredictable [1]–[4], can effectively overcome the shortcomings of conventional encryption methods [5]. Due to the advantages of spintronic devices, such as low power consumption and high endurance [6], [7], magnetic random-access memory (MRAM)-based PUFs which utilize variation in switching time, or sense current as the entropy source [8], [9] have been demonstrated. These PUFs can solve the deficiency of CMOS-based PUF [10]–[13] to a certain extent, but have fixed challenge-response pairs (CRPs) after fabrication. Reconfigurable PUF (rPUF) could be refreshed with updated CRPs which inherit all security properties [14]. Reconfigurability could enhance PUFs' resistance against exhaustive CRP access attacks and reliability deteriorations under extreme conditions [15]–[18].

Magnetic domain wall (DW) motion has been proposed for novel logic and memory devices [19]–[22]. However, the process variations make the DW pinning sites randomly distributed in devices which causes DW motion as well as nucleation time to be stochastic. This device-to-device (D2D) variation is undesirable in the DW based devices but is an ideal entropy source for PUF [23]–[25]. Moreover, the write cycle-to-cycle (C2C) variation makes the PUF reconfigurable. In this work, a reconfigurable PUF is demonstrated and proposed in Ta/CoFeB/MgO heterostructures, relying on spin-orbit torque (SOT) induced randomness of DW dynamics. The electrical measurements show that both D2D and C2C variation are observed after a current pulse flows through the Ta layer.

II. Device Structure and Manipulation of Magnetic Domain Wall Motion

The basic building block for our security hardware is implemented with 176 (22 × 8) micro-dot devices. The devices were fabricated from a stack of thermally oxidized Si (substrate)/Ta (10 nm)/CoFeB (1 nm)/MgO (1 nm)/Ta (2 nm). The optical image and the anomalous Hall effect (AHE) resistance (R_{AH}) as a function of out-of-plane magnetic fields of one single device with a size of 6 × 6 μm^2 are shown in Figure 1a. It shows that the device has a good perpendicular magnetic anisotropy with a coercivity of around 100 Oe. In addition, the SOT induced field-free R_{AH} switching is realized in our devices (Figure 1b), the mechanism will be discussed below.

We also investigated the C2C programming variation of the device and the D2D variation of 8 devices, as shown in Figure 1c and d, respectively. 100 cycles of tests with programming current pulses (amplitude in -9 MA/cm^2 for

Manuscript received January 8, 2021; accepted February 3, 2021. Date of publication February 8, 2021; date of current version March 24, 2021. This work was supported in part by the National Natural Science Foundation of China (NSFC) under Grant 62074063, Grant 61821003, Grant 61904051, Grant 61904060, Grant 51671098, and Grant 61674062; in part by the National Key Research and Development Program of China under Grant 2020AAA0109000; and in part by the Research Project of Wuhan Science and Technology Bureau under Grant 2019010701011394. The review of this letter was arranged by Editor B. Govoreanu. *(Corresponding author: Long You.)*

Zhen Cao, Shuai Zhang, Jian Zhang, Ruofan Li, Zhe Guo, Xiaofei Yang, Xuecheng Zou, and Jeongmin Hong are with the School of Optical and Electronic Information, Huazhong University of Science and Technology, Wuhan 430074, China.

Nuo Xu is with the Department of Electrical Engineering and Computer Sciences, University of California, Berkeley, CA 94720 USA.

Jijun Yun and Li Xi are with the Key Laboratory for Magnetism and Magnetic Materials of the Ministry of Education, Lanzhou University, Lanzhou 730000, China.

Min Song is with the Hubei Key Laboratory of Ferro and Piezoelectric Materials and Devices, Faculty of Physics and Electronic Science, Hubei University, Wuhan 430062, China.

Qiming Zou is with the Department of Electrical and Computer Engineering, University of Nebraska–Lincoln, Lincoln, NE 68588 USA.

Oukjae Lee is with the Center for Spintronics, Korea Institute of Science and Technology, Seoul 02792, South Korea.

Long You is with the School of Optical and Electronic Information, Huazhong University of Science and Technology, Wuhan 430074, China, and also with the Wuhan National Laboratory for Optoelectronics, Huazhong University of Science and Technology, Wuhan 430074, China (e-mail: lyou@hust.edu.cn).

Color versions of one or more figures in this letter are available at https://doi.org/10.1109/LED.2021.3057638.

Digital Object Identifier 10.1109/LED.2021.3057638

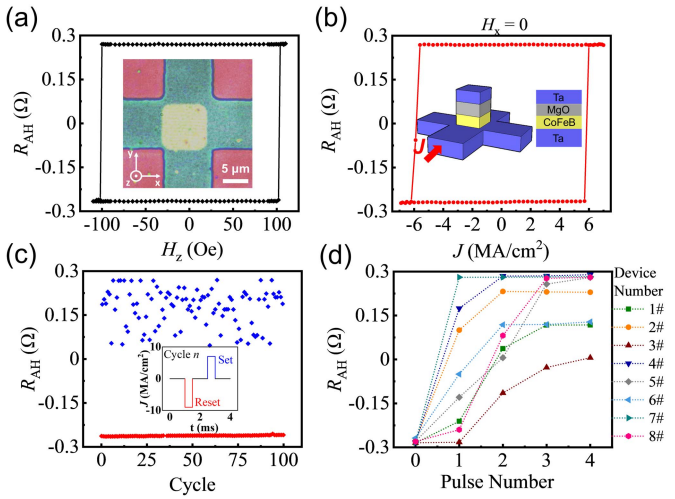

Fig. 1. (a) AHE loop with an inset of an optical image of the device. (b) SOT induced field-free switching. The inset shows FM layer stack which consists of Ta (10 nm)/CoFeB (1 nm)/MgO (1 nm)/Ta (2 nm) and the direction of the applied current to generate SOT and to detect AHE voltage. (c) The distribution of R_{AH} in 100 test cycles with the same device, the inset shows the applied current pulse of 1 cycle, amplitude in -9 or 7 MA/cm^2, duration in 500 μs. (d) R_{AH} evolutions after a fixed 7 MA/cm^2 / 300 μs current pulse is applied to 8 different devices.

Reset and 7 MA/cm^2 for Set, duration in 500 μs) for one device were performed, in which the device was firstly Reset at the beginning of each cycle. The Reset current (-9 MA/cm^2) are higher in magnitudes than the Set current (7 MA/cm^2), causing the magnet to reach its saturation state (red diamond in Figure 1c). Therefore, the C2C variation does not appear after Reset transition. The amplitude of Set pulse is too small to make the magnet reach its saturation state, the DW will be at a random position during programming. C2C variation is due to the different positions of the DWs in the same device after each Reset-Set operation. Therefore, refreshable CRPs based on C2C programming variations are implemented, and thus reconfigurable PUFs are constructed. While D2D variation originates from the different positions of DWs in each device after one Reset-Set operation, as shown in Figure 1d.

III. Cryptographic Functionality Implementation

In our PUF protocol, the challenges are the unit addresses and the responses are the corresponding binary codes. During the enrollment phase, a Set current pulse (around 650 μs duration and about 6.5 MA/cm^2 density) is applied to each device after Reset, then the R_{AH} value of each device on each unit (Figure 2a) is measured (Figure 2b). As shown in Figure 2c, the corresponding response for a given challenge can be obtained by the comparison method used the same as that in ref [13]. The collected CRPs will be stored in the database. In the authentication (response) phase, a challenge is selected from the stored database and presented to the PUF. If the PUF's response is close enough to the stored response, the device is deemed authentic. For reconfiguration, we Reset all the device, and a Set pulse is applied to each device. Due to the C2C variation (Figure 1c), the response will be changed under the same challenge. Furthermore, it is reported that after 10^{10} writing cycles, a DW motion based MRAM with CoFeB/MgO is still working with high performance [26]. In other words, the proposed PUF can be reconfigured by more than 10^{10} times.

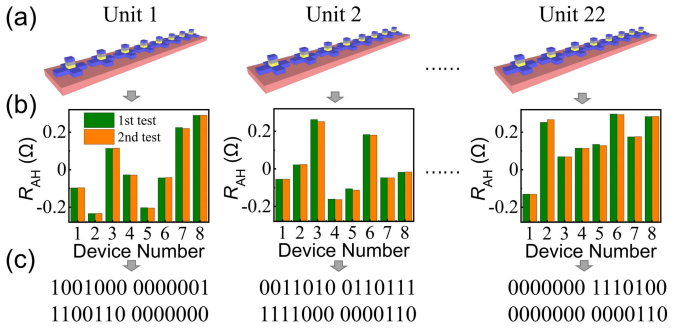

Fig. 2. (a) Illustration of device units used for the generation of cryptographic primitives. Each unit contains 8 micro-dot devices. (b) Distribution of R_{AH} after a current pulse is applied to different units. (c) 28-bit binary codes converted from analogy R_{AH} by the comparison method.

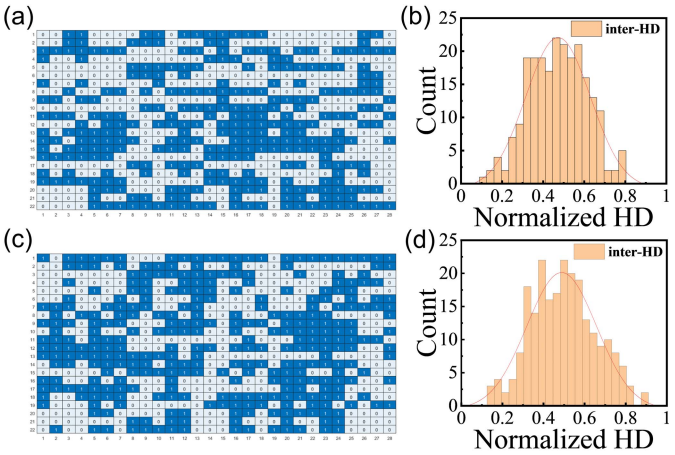

Fig. 3. (a), (c) 28 × 22 binary bits generated from R_{AH} by the comparison method before and after the reconfiguration respectively. (b), (d) Distributions of the normalized inter-HD before and after the reconfiguration respectively.

IV. Performance Evaluation

Figure 3a and 3c show the obtained bitmaps before and after reconfiguration, respectively. Then the uniqueness, bit-aliasing, uniformity and reliability are used to evaluate PUF's quality.

The uniqueness is characterized by inter- Hamming distance (HD), which can be derived from the distribution of the HD. Figure 3b and 3d show the distributions of the HD which is centered 0.488 and 0.472 before and after reconfiguration respectively, close to the ideal value (0.5).

In bit-aliasing, different device arrays produce nearly identical PUF responses. Bit-aliasing of the k-th bit of PUF is given by [27]

$$(Bit-aliasing)_k = \frac{1}{n}\sum_{i=1}^{n} r_{i,k}$$

where $r_{i,k}$ is the k-th bit of response from unit i. The Hamming Weight (HW) of the k-th bit in the unit i of the response across n units to assess the bit-aliasing of the k-th bit in the PUF. The idea value should be 0.5. In this work, the bit-aliasing is 0.530 and 0.497 before and after reconfiguration respectively.

The unpredictability of a PUF requires a high-quality uniformity. Uniformity is characterized by the proportion of "1" and "0" responses of a PUF, and the ideal proportion should be 50%. In our case, the uniformity distribution (measured by

the proportion of "1") is centered at 0.475 and 0.486 before and after reconfiguration respectively.

The reliability can be quantified by intra- HD which can be calculated as:

$$HD_{intra} = \frac{1}{m}\sum_{l=1}^{m}\frac{HD(t_1, t_2)}{n}$$

where t_1 and t_2 are the n-bit responses of two tests for the same device unit under varying conditions. The ideal intra-HD is 0. Regarding the effect of voltage variation, CRPs remain stable as long as the voltage is less than the critical voltage, which can cause the domain wall motion. In terms of temperature variation, according to the mechanism of AHE, the anomalous Hall resistivity, ρ_{AH}, is given by $\rho_{AH} = 4\pi R_S M_\perp$, where R_S is the AHE coefficient, $M_\perp$ is the magnetization along the perpendicular direction and equal to the saturation magnetization M_S for perpendicular magnetized films. Temperature dependence of magnetization follows the Bloch law which predicts $m_S(T) = m_S(0)\left(1 - BT^{3/2}\right)$, where $m_S(0)$ stands for the magnetization at 0 K, and B represents Bloch constant [28]. As a result, the relative R_{AH} values for all the devices which are made of same films would be invariable with temperature. It indicates the CRPs would remain the same with the temperature by using the comparison method.

V. Field-Free Switching Behavior

The process of DW motion and macro-spin flipping by SOT are illustrated in Fig. 4e, f. The hollow arrows in the free layer represent the direction of magnetization while the contours represent that around the domain wall region. When a charge current is flowing through the HM in the x-direction, a y-directional polarized spin current is injected into the free layer via the spin Hall effect which forms an effective magnetic field in the z direction, H_Z, and drives the DW along the x-direction.

As shown above, the magnetization in the present Ta/CoFeB/MgO system can be solely controlled by an electrical current, which is speculated as due to the formation of a chiral *Néel*-type DW [29], [30]. When an SOT current is applied to the device, reversed domains may be nucleated firstly with the assistance of *Joule* heating and then the newly generated DWs will propagate along or against the current flow direction under SOT, depending on the sign of spin Hall angle and the DMI effect of the Ta/CoFeB structure, until the complete domain flipping. Thus, the field-free switching can be achieved. Based on previous reports, right-handed chiral *Néel* walls are likely formed in our structure [31], [32].

Then the Dzyaloshinskii-Moriya Interaction (DMI) effective field (H_{DMI}) is estimated, whose magnitude determines the DW type (*Bloch* or *Néel* wall) [33]. The R_{AH} versus H_z loops are measured in the micro-dot device as a function of applied current (J) and H_x. Figure 4a shows R_{AH} vs H_z loops with $H_x = 1000$ Oe and $J = \pm 4$ MA/cm^2. These two AHE loops shift along the H_z axis, which define the H_Z^{eff} current-induced effective field H_Z^{eff}. From H_Z^{eff} Z plotted versus J (Figure 4b), H_Z^{eff} /J can be well estimated. The measured effective field per current density ($\chi = H_Z^{eff}/J$) as a function of H_x is summarized in Figure 4c. The χ increases quasi-linearly with H_x and saturates at $H_x \approx \pm 800$ Oe. Therefore, it can be estimated that $\chi_{sat} \approx 8.3$ Oe/ (MA/cm^2) and $|H_{DMI}| \approx 800$ Oe from the saturation value of χ and the saturation field, respectively.

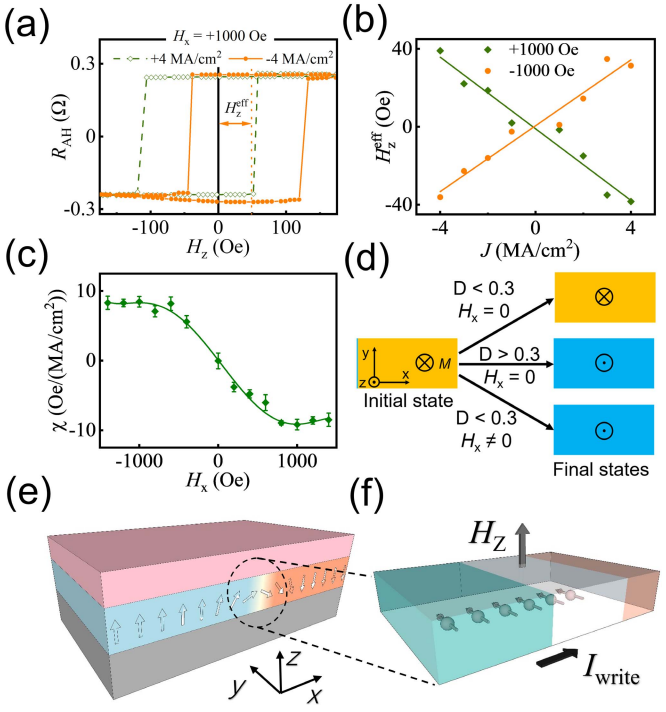

Fig. 4. (a) AHE loops at $J = \pm 4$ MA/cm^2 under an in-plane field $H_x = +1000$ Oe. (b) H_Z^{eff} as a function of J when $H_x = \pm 1000$ Oe. (c) Measured effective field versus current density under various in-plane fields. (d) Micro-magnetic simulations of SOT induced switching in three different cases. (e), (f) Magnetization dynamics induced by SOT.

The Object-Oriented Micro-Magnetic Framework (OOMMF) based micro-magnetic simulations were also performed, as shown in Fig. 4(d). We chose a 600 × 1200 nm^2 rectangular area, in which a reversed domain with a size of 600 × 40 nm^2 formed at the left edge with magnetization pointing up ($+z$ direction) and other area with magnetization pointing down (-z direction). A current of 10 MA/cm^2 is applied along x direction when changing DMI constant (D). The results show that when D is less than 0.3 mJ/m^2, the FM layer fails to switch at $H_x = 0$; while setting $H_x \neq 0$ or increasing $D > 0.3$ mJ/m^2, the switching occurs. In fact, chiral *Néel*-type DWs will be stabilized if D is large enough. D was estimated from $H_{DMI} = D/(\mu_0 M_s \Delta)$ [34], $M_S = 1.16 \times 10^6$ A/m and Δ is the DW width obtained from $\Delta = \sqrt{A/K_{eff}}$, $A = 30$ pJ/m, $K_{eff} = 5.8 \times 10^5$ J/m^3. D of the devices is around 0.65 mJ/m^2, which is above 0.3 mJ/m^2. Therefore, in addition to the experimental results, this simulation has confirmed our assumption that the SOT induced field-free switching is ascribed to the generation of chiral *Néel*-type DWs.

VI. Conclusion

We have reported a reconfigurable PUF in a Ta/CoFeB/MgO multilayered structure, which is demonstrated by SOT induced field-free and stochastic DW motion. The spatial variation of DW in such a device makes it feasible for a PUF, while the repeating current pulses can reconfigure the PUF's state. The good performance parameters prove that the scheme is feasible. Furthermore, SOT induced field-free switching is also realized, which is likely attributed to the large DMI coefficient of the films. The DW motion based PUF process is also favorable for low-temperature CMOS-BEOL integrations to construct 3D and high-density PUF arrays.

REFERENCES

[1] R. Pappu, B. Recht, J. Taylor, and N. Gershenfeld, "Physical one-way functions," *Science*, vol. 297, no. 5589, pp. 2026–2030, Sep. 2002, doi: 10.1126/science.1074376.

[2] J. D. R. Buchanan, R. P. Cowburn, A. V. Jausovec, D. Petit, P. Seem, G. Xiong, D. Atkinson, K. Fenton, D. A. Allwood, and M. T. Bryan, "'Fingerprinting' documents and packaging," *Nature*, vol. 436, no. 7050, p. 475, Jul. 2005, doi: 10.1038/436475a.

[3] R. Horstmeyer, B. Judkewitz, I. M. Vellekoop, S. Assawaworrarit, and C. Yang, "Physical key-protected one-time pad," *Sci. Rep.*, vol. 3, no. 1, p. 3543, Dec. 2013, doi: 10.1038/srep03543.

[4] C. Herder, M.-D. Yu, F. Koushanfar, and S. Devadas, "Physical unclonable functions and applications: A tutorial," *Proc. IEEE*, vol. 102, no. 8, pp. 1126–1141, Aug. 2014, doi: 10.1109/JPROC.2014.2320516.

[5] U. R Ührmair, F. Sehnke, J. S Ölter, G. Dror, S. Devadas, and J. Ü. Schmidhuber, "Modeling attacks on physical unclonable functions," in *Proc. 17th ACM Conf. Comput. Commun. Secur. (CCS)*, 2010, pp. 237–249, doi: 10.1145/1866307.1866335.

[6] K. Yue, Y. Liu, R. K. Lake, and A. C. Parker, "A brain-plausible neuromorphic on-the-fly learning system implemented with magnetic domain wall analog memristors," *Sci. Adv.*, vol. 5, no. 4, Apr. 2019, Art. no. eaau8170, doi: 10.1126/sciadv.aau8170.

[7] W. A. Borders, A. Z. Pervaiz, S. Fukami, K. Y. Camsari, H. Ohno, and S. Datta, "Integer factorization using stochastic magnetic tunnel junctions," *Nature*, vol. 573, no. 7774, pp. 390–393, Sep. 2019, doi: 10.1038/s41586-019-1557-9.

[8] A. Kumar, S. Sahay, and M. Suri, "Switching-time dependent PUF using STT-MRAM," in *Proc. 31st Int. Conf. VLSI Design, 17th Int. Conf. Embedded Syst. (VLSID)*, Jan. 2018, pp. 434–438, doi: 10.1109/VLSID.2018.103.

[9] E. I. Vatajelu, G. D. Natale, M. Indaco, and P. Prinetto, "STT MRAM-based PUFs," in *Proc. Design, Autom. Test Eur. Conf. Exhib. (DATE)*, 2015, pp. 872–875, doi: 10.7873/DATE.2015.0505.

[10] S. Morozov, A. Maiti, and P. Schaumont, "An analysis of delay based PUF implementations on FPGA," in *Proc. Int. Symp. Appl. Reconfigurable Comput.*, Mar. 2010, pp. 382–387, doi: 10.1007/978-3-642-12133-3_37.

[11] J. Guajardo, S. S. Kumar, G.-J. Schrijen, and P. Tuyls, "FPGA intrinsic PUFs and their use for IP protection," in *Proc. Cryptograph. Hardw. Embedded Syst. (CHES)*, Sep. 2007, pp. 63–80, doi: 10.1007/978-3-540-74735-2_5.

[12] D. Lim, J. W. Lee, B. Gassend, G. E. Suh, M. van Dijk, and S. Devadas, "Extracting secret keys from integrated circuits," *IEEE Trans. Very Large Scale Integr. (VLSI) Syst.*, vol. 13, no. 10, pp. 1200–1205, Oct. 2005, doi: 10.1109/TVLSI.2005.859470.

[13] H. Chen, M. Song, Z. Guo, R. Li, Q. Zou, S. Luo, S. Zhang, Q. Luo, J. Hong, and L. You, "Highly secure physically unclonable cryptographic primitives based on interfacial magnetic anisotropy," *Nano Lett.*, vol. 18, no. 11, pp. 7211–7216, Oct. 2018, doi: 10.1021/acs.nanolett.8b03338.

[14] K. Kursawe, A.-R. Sadeghi, D. Schellekens, B. Skoric, and P. Tuyls, "Reconfigurable physical unclonable functions–enabling technology for tamper-resistant storage," in *Proc. IEEE Int. Workshop Hardw.-Oriented Secur. Trust*, Jul. 2009, pp. 22–29, doi: 10.1109/HST.2009.5225058.

[15] A. Chen, "Utilizing the variability of resistive random access memory to implement reconfigurable physical unclonable functions," *IEEE Electron Device Lett.*, vol. 36, no. 2, pp. 138–140, Feb. 2015, doi: 10.1109/LED.2014.2385870.

[16] L. Zhang, Z. Hui Kong, C.-H. Chang, A. Cabrini, and G. Torelli, "Exploiting process variations and programming sensitivity of phase change memory for reconfigurable physical unclonable functions," *IEEE Trans. Inf. Forensics Security*, vol. 9, no. 6, pp. 921–932, Jun. 2014, doi: 10.1109/TIFS.2014.2315743.

[17] Y. Pang, B. Gao, D. Wu, S. Yi, Q. Liu, W.-H. Chen, T.-W. Chang, W.-E. Lin, X. Sun, S. Yu, H. Qian, M.-F. Chang, and H. Wu, "25.2 A reconfigurable RRAM physically unclonable function utilizing post-process randomness source with $<6\times10^{-6}$ native bit error rate," in *IEEE Int. Solid-State Circuits Conf. (ISSCC) Dig. Tech. Papers*, Feb. 2019, pp. 402–404, doi: 10.1109/ISSCC.2019.8662307.

[18] A. Chen, "Reconfigurable physical unclonable function based on probabilistic switching of RRAM," *Electron. Lett.*, vol. 51, no. 8, pp. 615–617, Apr. 2015, doi: 10.1049/el.2014.4375.

[19] D. A. Allwood, G. Xiong, C. C. Faulkner, D. Atkinson, D. Petit, and R. P. Cowburn, "Magnetic domain-wall logic," *Science*, vol. 309, no. 5741, pp. 1688–1692, Sep. 2005, doi: 10.1126/science.1108813.

[20] D. A. Allwood, G. Xiong, M. D. Cooke, C. C. Faulkner, D. Atkinson, N. Vernier, and R. P. Cowburn, "Submicrometer ferromagnetic NOT gate and shift register," *Science*, vol. 296, no. 5575, pp. 2003–2006, Jun. 2002, doi: 10.1126/science.1070595.

[21] D. Atkinson, D. S. Eastwood, and L. K. Bogart, "Controlling domain wall pinning in planar nanowires by selecting domain wall type and its application in a memory concept," *Appl. Phys. Lett.*, vol. 92, no. 2, Jan. 2008, Art. no. 022510, doi: 10.1063/1.2832771.

[22] S. S. P. Parkin, M. Hayashi, and L. Thomas, "Magnetic domain-wall racetrack memory," *Science*, vol. 320, no. 5873, pp. 190–194, Apr. 2008, doi: 10.1126/science.1145799.

[23] G. Meier, M. Bolte, R. Eiselt, B. Krüger, D.-H. Kim, and P. Fischer, "Direct imaging of stochastic domain-wall motion driven by nanosecond current pulses," *Phys. Rev. Lett.*, vol. 98, no. 18, May 2007, Art. no. 187202, doi: 10.1103/PhysRevLett.98.187202.

[24] E. Martinez, "The stochastic nature of the domain wall motion along high perpendicular anisotropy strips with surface roughness," *J. Phys., Condens. Matter*, vol. 24, no. 2, Dec. 2011, Art. no. 024206, doi: 10.1088/0953-8984/24/2/024206.

[25] A. Iyengar, K. Ramclam, and S. Ghosh, "DWM-PUF: A low-overhead, memory-based security primitive," in *Proc. IEEE Int. Symp. Hardware-Oriented Secur. Trust (HOST)*, May 2014, pp. 154–159, doi: 10.1109/HST.2014.6855587.

[26] T. Suzuki, H. Tanigawa, Y. Kobayashi, K. Mori, Y. Ito, Y. Ozaki, K. Suemitsu, T. Kitamura, K. Nagahara, E. Kariyada, N. Ohshima, S. Fukami, M. Yamanouchi, S. Ikeda, M. Hayashi, M. Sakao and H. Ohno, "Low-current domain wall motion MRAM with perpendicularly magnetized CoFeB/MgO magnetic tunnel junction and underlying hard magnets," in *Proc. Symp. VLSI Technol.*, Jun. 2013, pp. T138–T139.

[27] A. Maiti, J. Casarona, L. McHale, and P. Schaumont, "A large scale characterization of RO-PUF," in *Proc. IEEE Int. Symp. Hardw.-Oriented Secur. Trust (HOST)*, Anaheim, CA, USA, Jun. 2010, pp. 94–99, doi: 10.1109/HST.2010.5513108.

[28] S. B. Wu, T. Zhu, X. F. Yang, and S. Chen, "The anomalous Hall effect in the perpendicular Ta/CoFeB/MgO thin films," *J. Appl. Phys.*, vol. 113, no. 17, Mar. 2013, Art. no. 17C717, doi: 10.1063/1.4796192.

[29] S. Emori, U. Bauer, S.-M. Ahn, E. Martinez, and G. S. D. Beach, "Current-driven dynamics of chiral ferromagnetic domain walls," *Nature Mater.*, vol. 12, no. 7, pp. 611–616, Jun. 2013, doi: 10.1038/nmat3675.

[30] J. Torrejon, J. Kim, J. Sinha, S. Mitani, M. Hayashi, M. Yamanouchi, and H. Ohno, "Interface control of the magnetic chirality in CoFeB/MgO heterostructures with heavy-metal underlayers," *Nature Commun.*, vol. 5, no. 1, pp. 1–8, Aug. 2014, doi: 10.1038/ncomms5655.

[31] S. Zhang, S. Luo, N. Xu, Q. Zou, M. Song, J. Yun, Q. Luo, Z. Guo, R. Li, W. Tian, X. Li, H. Zhou, H. Chen, Y. Zhang, X. Yang, W. Jiang, K. Shen, J. Hong, Z. Yuan, L. Xi, K. Xia, S. Salahuddin, B. Dieny, and L. You, "Memristors: A spin–orbit-torque memristive device (adv. electron. mater. 4/2019)," *Adv. Electron. Mater.*, vol. 5, no. 4, Apr. 2019, Art. no. 1970022, doi: 10.1002/aelm.201970022.

[32] J. Cao, Y. Chen, T. Jin, W. Gan, Y. Wang, Y. Zheng, H. Lv, S. Cardoso, D. Wei, and W. S. Lew, "Spin orbit torques induced magnetization reversal through asymmetric domain wall propagation in Ta/CoFeB/MgO structures," *Sci. Rep.*, vol. 8, no. 1, pp. 1–9, Jan. 2018, doi: 10.1038/s41598-018-19927-5.

[33] C.-F. Pai, M. Mann, A. J. Tan, and G. S. D. Beach, "Determination of spin torque efficiencies in heterostructures with perpendicular magnetic anisotropy," *Phys. Rev. B, Condens. Matter*, vol. 93, no. 14, Apr. 2016, Art. no. 144409, doi: 10.1103/PhysRevB.93.144409.

[34] A. Thiaville, S. Rohart, É. Jué, V. Cros, and A. Fert, "Dynamics of dzyaloshinskii domain walls in ultrathin magnetic films," *EPL, Europhys. Lett.*, vol. 100, no. 5, p. 57002, Dec. 2012, doi: 10.1209/0295-5075/100/57002.